Journal of Geomorphology
Stuttgart, May 2023

Quantitative long-term (1922 to 2021) monitoring of a large-scale landslide of a LIA lateral moraine due to glacial debuttressing

Moritz Altmann[1,*], Florian Haas[1], Jakob Rom[1], Fabian Fleischer[1], Tobias Heckmann[1], Camillo Ressl[2], Michael Becht[1]

[1] Department of Physical Geography, Catholic University of Eichstätt-Ingolstadt, Eichstätt, 85072, Germany
[2] Department of Geodesy and Geoinformation, TU Wien, Vienna, 1040, Austria
* Corresponding author: Maltmann@ku.de

With 9 figures and 3 tables

Abstract: We present a 99-year monitoring (1922 to 2021) of a large-scale deformation of the terminal part of a Little Ice Age lateral moraine in the glacier forefield of the Gepatschferner in the Upper Kaunertal in Tyrol, Austria. The reconstruction of this large-scale landslide was carried out in high temporal and spatial resolution using 12 DEMs of differences based on 13 different Digital elevation models from several epochs and remote sensing techniques. These were generated from a stereo photogrammetric map (1922), historical aerial photographs (between 1953 and 2003) using structure-from-motion photogrammetry with multi-view-stereo and airborne Light Detection and Ranging data (between 2006 and 2021). Based on the analysis of the different epochs, the period of the main landslide could be dated between 1953 and 1971. However, landslides were detected in all the first three epochs (1922 to 1953, 1953 to 1971 and 1971 to 1983), covering a period of 61 years. In the epoch of the main landslide, there was a vertical and horizontal displacement of about 70 and 100 m, respectively, while the landslide was about 190 m wide, which results in a calculated volume of 287,537 (±2,026) m^3. We assume that the instability of the slope was caused by glacial debuttressing due to the glacier retreat since the end of the Little Ice Age. During the entire period, the slope was subject to strong variations in geomorphological activity, both spatially and temporally. The landslide area shows continuous geomorphological activity over the entire study period (1922 to 2021), summing up the total volume of net erosion to about 486,000 m^3.

Keywords: Airborne light detection and ranging; historical aerial photos; large-scale landslide; Little Ice Age lateral moraine; long-term change detection; structure-from-motion photogrammetry with multi-view-stereo; historical stereo photogrammetric map

1 Introduction

In recent decades, global warming has led to rapid landscape changes, especially in sensitive and vulnerable areas such as high mountain regions (Hock et al. 2019). Lateral moraines within proglacial areas (Schiefer & Gilbert 2007), which were exposed after the glacial maximum of the Little Ice Age (LIA) around the mid-20th century (Matthews & Briffa 2005, Ivy-Ochs et al. 2009), often show high slope instability within the phase of the paraglacial adjustment process, which can extend to several decades and centuries (Ballantyne 2002a, b, Deline et al. 2015, Haeberli et al. 2017, Heckmann & Morche 2019). On the steep slopes, this can lead to the formation of deeply incised gully systems, mainly caused by fluvial erosion, nival processes and debris flows (Ballantyne & Benn 1994, Curry et al. 2006, Betz-Nutz et al. 2023). In addition, slope deformations such as landslides occur, which may be related to the retreat of glaciers and the associated destabilisation of the connected slopes, which is described as glacial debuttressing. Such a destabilisation may occur immediately after ice loss or decades later, e.g. due to heavy rainfall events (Mattson & Gardner 1991, Blair 1994, Stoffel et al. 2014, Altmann et al. 2020, Cody et al. 2020). At the Fox Glacier in the Te Moeka o Tuawe Valley in New Zealand, Cody et al. (2020) showed, using high temporal resolution daily time-lapse imagery and pixel tracking between 2014 and

DOI: 10.1127/jgeomorphology/2023/0779

Gebrüder Borntraeger Science Publishers, Stuttgart, www.borntraeger-cramer.de

2018, that internal deformation of the slope by slow sliding is directly related to the glacier retreat. It was also observed that rotational sliding was reworked after glacier melt due to debris flows triggered by rainfall events. In addition, Hugenholtz et al. (2008) described a large-scale deformation of the eastern lateral moraine of the Athabasca Glacier in Jasper National Park (Alberta, Canada) that began in the early 1950s and deformed mainly in the late 1960s. The slide involves a 41 m vertical and 55 m horizontal displacement of a 540 m long lateral moraine section towards the glacier forefield. Vibrations from road traffic or the impact of a rock glacier in the area behind are mentioned as possible triggers. Stoffel & Huggel (2012) demonstrated instead that in 2009 a landslide occurred on a lateral moraine at the glacial lake of the Lower Grindelwald glacier (Switzerland). Emmer et al. (2020) showed, in the glacier forefield of the Kinzl Glacier (Peruvian Cordillera Blanca), over a period of several decades (since 1932 to 2016), using historical photographs, remotely sensed images and field observations, the occurrence of a total of 25 landslides, which are directly or indirectly attributable to the glacier retreat. However, the few existing studies show the rarity of such processes and also the corresponding particularities in individual cases.

In order to investigate landscape evolution in high alpine areas, Airborne Laser Scanning (ALS) offers several advantages, as it allows e.g. a very accurate survey of the Earth's surface (Bollmann et al. 2011, Sailer et al. 2012, Guo et al. 2021, Stark et al. 2022). Thus, based on Digital elevation models (DEM) over at least two time periods, topographic changes can be quantitative detected and interpreted by calculating a DEM of Difference (DoD) (James et al. 2012, Williams 2012, Hilger 2017). In addition, historical aerial photographs processed to DEMs using structure-from-motion (SfM) photogrammetry with multi-view-stereo (MVS) provide effective opportunities to extend the quantitative study period of topographic changes to several decades (Lane et al. 2017, Altmann et al. 2020, Fleischer et al. 2021, Piermattei et al. 2022, Stark et al. 2022). However, the temporal coverage of aerial photographs, e.g. of the European Alps, only extends to about the middle of the 20th century, which leads to a temporal limitation of these studies. Fleischer et al. (2022) showed another possibility to extend the study period for quantitative studies of high alpine areas by analysing the acceleration of a rock glacier, using contour lines of a historical map (from 1922) by transferring them to a DEM and comparing them with later DEMs (from the 1950s onwards based on aerial photographs and LiDAR Data).

Therefore, the aim of this study is to show a quantitative long-term reconstruction of the topographic volume changes of a large-scale landslide in a proglacial area. To ensure the longest possible study period, we use not only topographic remote sensing data such as current airborne LiDAR data (from 2006 to 2021) and historical aerial photographs (between 1953 and 2003), but also a historical map (from 1922). We thus present an approach to quantify the corresponding morphodynamics in proglacial areas over a period of almost 100 years, covering several decades before the 1950s, from which the first aerial photos of the European Alps are mostly available, limiting the study period of several studies. Due to the high spatial (1×1 m) and temporal (13 DEMs/12 DoDs) resolution of the study area, another objective of this study is to classify the temporal sequence of this deformation and to identify differences in the magnitude and frequency of the corresponding geomorphological activity. In addition, the glacier extents of the study area were mapped and the influence of the glacier retreat on the morphodynamic of the slope was investigated. Finally, this study contributes to a better understanding of the paraglacial adjustment process and thus demonstrates the response of a slope to the glacier retreat within a proglacial area.

2 Study area

The study site is located in the glacier forefield of the Gepatschferner (Gepatsch glacier), which belongs to the Upper Kaunertal (Kauner Valley) in Tyrol (Austria), in the Ötztal Alps, a part of the central Eastern Alps. The Kaunertal is a north-south oriented valley bordering the main Alpine ridge and Italy in the south. Geologically, the upper Kaunertal belongs to the Austroalpine crystalline complex (Geological Survey of Austria 1999). Bedrock lithology such as crystalline rocks, mainly ortho- and paragneisses, dominate (Hilger 2017). Due to its inner-alpine location and the corresponding protective effect of the surrounding mountain ranges, a continental climate prevails with comparatively low mean annual precipitation, which makes it one of the driest regions in the Alps (inner-alpine dry region) (Hilger 2017). The Gepatschferner experienced a strong retreat in the recent decades. After the maximum glacier extent in 1856 (Nicolussi & Kerschner 2014) at the end of LIA, there was a continuous melting with few exceptions were minor advances occur, such as in the years 1920/1921 and between 1977 and 1988 (Nicolussi & Kerschner 2014). Due to the strong glacier retreat, the main outlet of the Gepatschferner melted by about 3 km between 1856 and 2021. After deglaciation, the glacier forefield of the Gepatschferner has been shaped by a variety of different geomorphological processes in the last decades. Fluvial and nival erosion processes, landslides and debris flows, are the predominant processes. Thus, some sections of

the lateral moraine show strongly incised gullies, with high erosion rates during the last decades (Altmann et al. 2020, Betz-Nutz et al. 2022, Altmann et al. 2023). However, several studies show a decrease in geomorphological activity of the lateral moraines, such as Altmann et al. (2020), Betz-Nutz et al. (2022), Stark et al. (2022) and Altmann et al. (2023) from the 1950s/1970s to 2019. The Fagge River, which drains the glacier forefield, shows an aggradation and balance of sediment (from 1953 onwards) until the late 1990s, followed by a deterioration tendency of the sediment balance since the 2000s until 2019 (especially from 2003 onwards) (Piermattei et al. 2022). Thus, the Area of Interest (AoI) is characterised by intense morphodynamics, low vegetation cover and typical moraine material (Fig. 1). The AoI ranges, with a difference of 180 m, from an elevation of 2235 to 2415 m (ellipsoidal heights) and covers an area of 4.4 ha. With a northeast aspect, a mean slope gradient of 34.9° is reached (maximum slope gradient is 62.8°). The maximum length of the delineated AoI measures 273.2 m.

3 Material and methods

3.1 Material

To achieve the objectives of this study, both historical and modern topographic datasets from different remote sensing techniques were processed and combined. For the second half of the 19th century and the first half of the 20th century, historical maps were considered. From the second half of the 20th century onwards, historical aerial photographs (1953 to 2003) were taken and processed into high-resolution DEMs. In addition, airborne LiDAR data from 2006 to 2021 were included (Fig. 2, Table 1, 2 and 3).

3.2 Methods

3.2.1 Generation of DEMs based on historical maps, historical aerial photographs and airborne LiDAR data

The DEM generation of the stereo photogrammetrically recorded historical map of 1922, which shows the entire Upper Kaunertal and was published by Finsterwalder (1928), was performed according to the approach developed by Fleischer et al. (2022). For this purpose, the digitised map (contour lines with an equidistance of 20 m) was georeferenced to the LiDAR-based DEM of 2017 (Table 3), which was available in the coordinate system ETRS89/UTM Zone 32N (EPSG code: 25832). In a first step, the mean elevation difference of the two data sets (based on 17 points) was determined. In a second step, the elevation value of the DEM from 2017 was adjusted so that the elevation information matches the historical map. Based on this, contour lines (with the same equidistance as the historical map) were created for the 2017 DEM, which thus fit the contour lines of the historical map. The georeferencing of the historical map to the 2017 DEM was then performed using the Adjust transformation method (Fleischer et al. 2022) at a total of 305 clearly identifiable and evenly distributed co-registration points on these contour lines (RMSE 1.7 m). The contour lines of the georeferenced map were then vectorised manually. These were then generated to a DEM (5 m) using the Topo to Grid tool ANUDEM in Esri ArcMap (version 10.6.1) and corrected for the previously determined height difference. In addition, the entire 1922 DEM was co-registered with the unmodified 2017 DEM using the Python tool pybob (McNabb 2019).

This approach was applied to another historical map, mapped in 1886 and 1887 (contour lines with an equidistance of 10 m) by Finsterwalder & Schunck (1888) (Table 1). However, the survey was not done stereo photogrammetrically but by trigonometric measurements of several points in the terrain using a theodolite. The map was additionally completed by 13 photographs and 30 terrain sketches. However, the accuracy and precision of the DEM (part of the AoI) was not sufficient to compare it with the other DEMs in order to determine quantitative surface changes back to 1886/1887. The sections of the AoI of both maps are shown in Fig. 3.

Scanned historical aerial photo series were photogrammetrically processed to generate corresponding high-resolution historical DEMs (1 m resolution) using structure-from-motion (SfM) with multi-view-stereo (MVS). For this purpose Agisoft Metashape Professional (Version 1.6.6; Agisoft LLC) was used and Trimble Inpho (Version 9.2) for the 2003 aerial photo series, as better results could be obtained in this case. For a detailed description of the workflow please refer to Altmann et al. (2020) and Stark et al. (2022).

Furthermore, LiDAR data sets from the years 2006 to 2021 (Table 3) were processed into DEMs. For a detailed description of these data, the sources and the corresponding workflow of these, please refer to Stark et al. (2022) and Piermattei et al. (2022). To generate the DEMs, the point clouds were processed in SAGA-LIS with Point Cloud to Grid. The elevation of the points was averaged for each grid cell (cell size 1 m). Prior to this conversion, vegetation filtering (ground classification), removal of outliers (Remove Isolated Points) and thinning of the point clouds (3D Block Thinning) were conducted. In order to get the highest possible precision and accuracy of the DoDs based on the corresponding DEMs, all point clouds were also georeferenced to the 2017 point cloud (due to the highest quality of all topographic datasets), based on stable areas, using the Iterative Closest Point

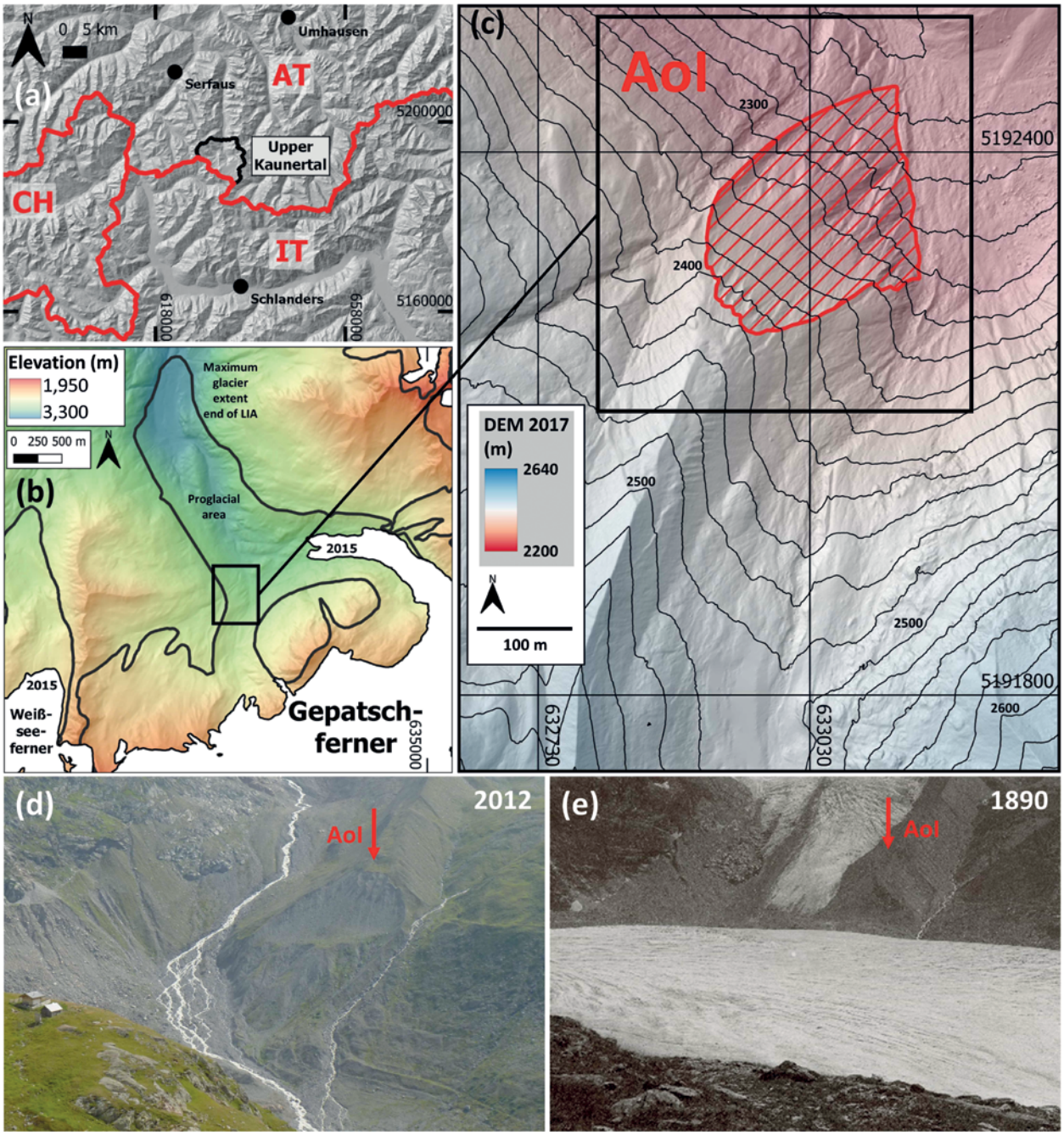

Fig. 1. Location of the study area (AoI) in the glacier forefield of the Gepatschferner in the Upper Kaunertal (Tyrol, Austria) **(a-c)** as well as a photo of the AoI from **(d)** 2012 (taken by Michael Becht) and a historical photo from **(e)** 1890 (Source: Landesarchiv Salzburg/Würthle and Spinnhirn). Sources of the glacier extents: End of LIA: Groß & Patzelt (2015), 2015: Buckel & Otto (2018). Large-scale hillshade (25 m) **(a)** based on SRTM and ASTER GDEM (Copernicus 2016). High resolution DEM (b and c) based on Airborne LiDAR data from 2017 (Table 3). Used coordinate system: ETRS89/UTM Zone 32N, EPSG Code: 25832.

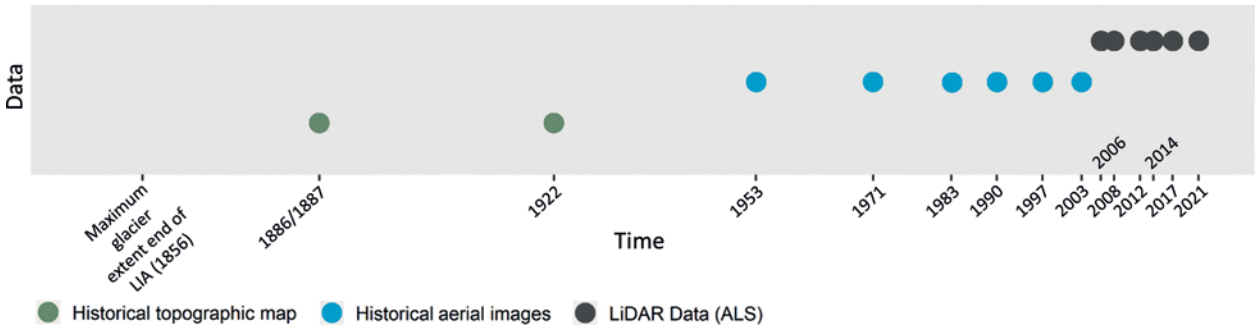

Fig. 2. Temporal overview of the processed data.

Table 1. Attributes of the historical maps.

Date of recording	Created by	Published map	Source and description	Scale	Contour lines	Method
2.-15.8.1886 and 2.-14.8.1887	Finsterwalder, S.; Schunck, H. and Blümcke, A.	Die Zunge des Gepatsch-Ferners	(Finsterwalder & Schunck 1888)	N/A	10 m	Trigonometric measurements using a the-odolite (plus 13 images and 30 terrain sketches)
Mid-August 1922 (12 days)	Ulrich, S.; Finsterwalder, R.; Sartorius, J.	Der Talschluß des Kaunsertales in den Oetztaleralpen mit dem Gepatsch- u. Weißseeferner	(Finsterwalder 1928)	Published in 1:20.000 (original created in 1:10.000)	Published with 20 m (original created with 10 m)	Sterophoto-grammetric (with 17 photo-graphs using a phototheodolite)

Table 2. Attributes of the historical aerial photographs. * The entire catchment area of the Upper Kaunertal was processed with the corresponding images (entire available image data set of the overflight).

Date of recording	Source/Purpose and designation	Images*	Camera Model, Band	Focal length [mm]	Flying Altitude [m a.s.l.]	Type/ Scanning resolution (µm)	Result and resolution	Mean point density of AoI (pts./m²)
05.06./31.8. and 08.09.1953	BEV/Forest condition estimation, C	124	Wild RC5, BW	210.1	ca. 3330	film/15	DEM (1 m)	7.1
18.08.1971	Land Tirol/ Overall flight Tyrol	91	Wild RC5/ RC8, BW	209.5	ca. 3080	film/12	DEM (1 m)	13.5
24.09.1983	BEV/Kaunertal	7	Wild RC10, BW	152.6	ca. 4840	film/15	DEM (1 m)	9.5
10.10.1990	BEV/KF 171-173	35	Wild RC10, BW	152.6	ca. 5850	film/15	DEM (1 m)	1.5
11.09.1997	BEV/KF 173	25	Wild RC10, BW	152.7	ca. 6010	film/15	DEM (1 m)	1.3
05.09.2003	BEV/Ötztaler Alpen/Oberinntal	59	N/A, RGB	305.1	ca. 4800	film/15	DEM (1 m)	0.59

Table 3. Attributes of the airborne LiDAR Data.

Date of recording	Operator/Source	Scanner	Wave length (nm)	Result and resolution	Mean point density (AoI) (pts./m²)
05.09.2006	Land Tirol (BSF Swissphoto AG)	ALTM 3100/ Gemini (Optech Inc., Canada)	999	DEM, 1 m	5.2
09.09.2008	Land Tirol (BSF Swissphoto AG)	ALTM 3100/ Gemini (Optech Inc., Canada)	999	DEM, 1 m	7
18.07.2012	Milan Geoservice GmbH (commissioned)	Riegl LMSQ 680i-S	1064	DEM, 1 m	15
18.07.2014	Milan Geoservice GmbH (commissioned)	Riegl LMS-VQ580	1064	DEM, 1 m	11.5
05.07.2017	Chair of Physical Geography, Catholic University of Eichstätt-Ingolstadt	VP1 (Riegl VuxSys-LR)	1550	DEM, 1 m	23.4
23.09.2021	Chair of Physical Geography, Catholic University of Eichstätt-Ingolstadt	VP1 (Riegl VuxSys-LR)	1550	DEM, 1 m	21.3

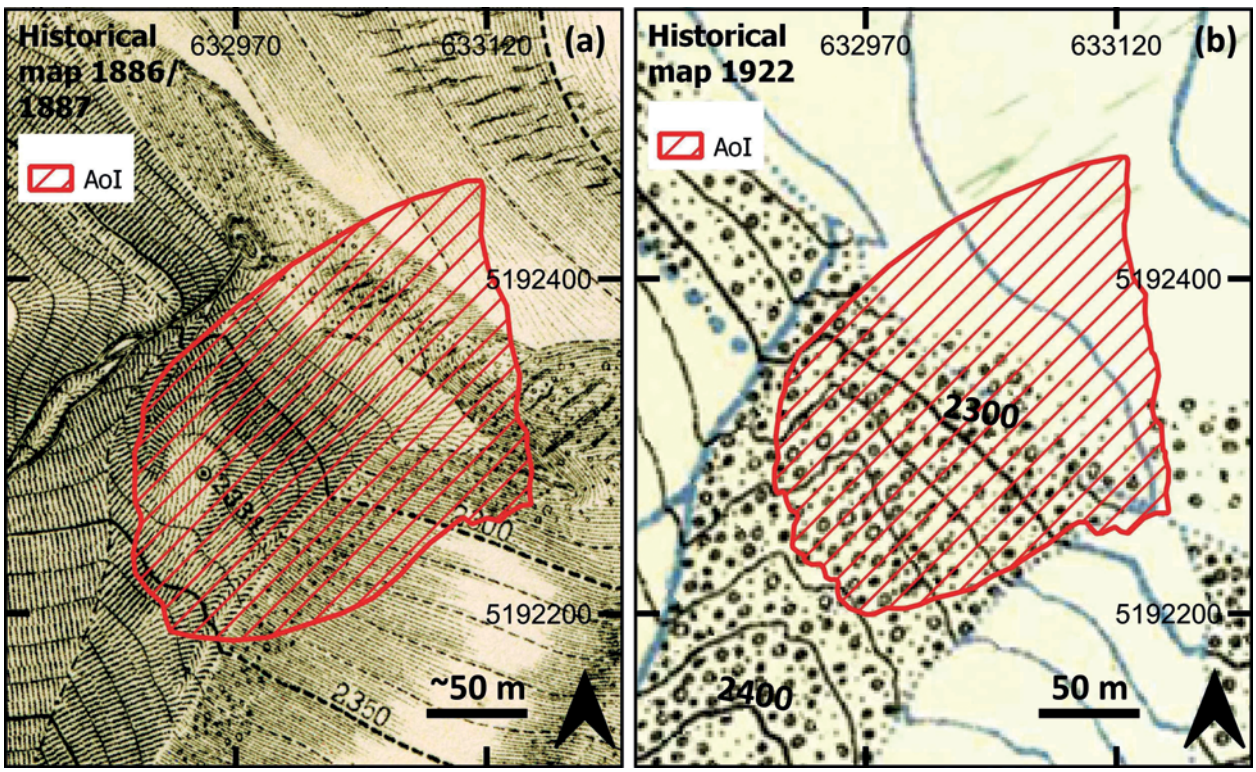

Fig. 3. Section of the AoI of the historical map from **(a)** 1886/1887 (Finsterwalder & Schunck 1888) and **(b)** 1922 (Finsterwalder 1928). The determination of the AoI in the 1886/1887 map was slightly adjusted. Additionally, elevation data were added to the 1922 map.

algorithm (ICP) (Besl & McKay 1992, Bakker & Lane 2017) in SAGA-LIS.

3.2.2 DEM of Difference (DoD) generation and volume calculations with error assessment

To determine the volume change of the Earth's surface of each epoch, the DEMs were computed to DoDs by subtracting them accordingly using SAGA-GIS (cell-value DEM_1 – cell-value DEM_2 = cell-value DoD). The erosion areas were mapped and all values (positive and negative) of this area within the AoI were summed up using the following equation (1):

$$\text{Volume} = \Sigma\text{DoD} * L^2 \quad (1)$$

where ΣDoD is the sum of all DoD values and L^2 the cell size (in this case 1 m).

The determination of the error range of the calculated volume changes of the geomorphologically active areas was done following Anderson (2019), who shows how corresponding uncertainties of net changes based on repeating topographic measurements can be estimated. Accordingly, the uncorrelated, correlated and systematic error of the DoDs were determined using a nearby stable area (blue hatched in Fig. 6, with a size of 11,925 m²) and the total error of the determined volume change as calculated using the following formula: Eq. (2):

$$\sigma_v = \sqrt{\sigma_{v,re}^2 + \sigma_{v,sc}^2 + \sigma_{v,sys}^2} \quad (2)$$

where $\sigma_{v,re}$ is the uncorrelated error, $\sigma_{v,sc}$ the spatially correlated error and $\sigma_{v,sys}$ the systematic error.

As suggested by Anderson (2019), the application of a threshold (level of detection) to separate actual changes from errors was omitted. Fig. 4 shows the standard deviation, the RMSE, the mean value, the maximum value and the minimum value of the stable area of the respective epoch.

When calculating the error range of the calculated volume change of the AoI within the first epoch (using the 1953/1922 DoD), an additional correction factor was determined to estimate the transformation uncertainties

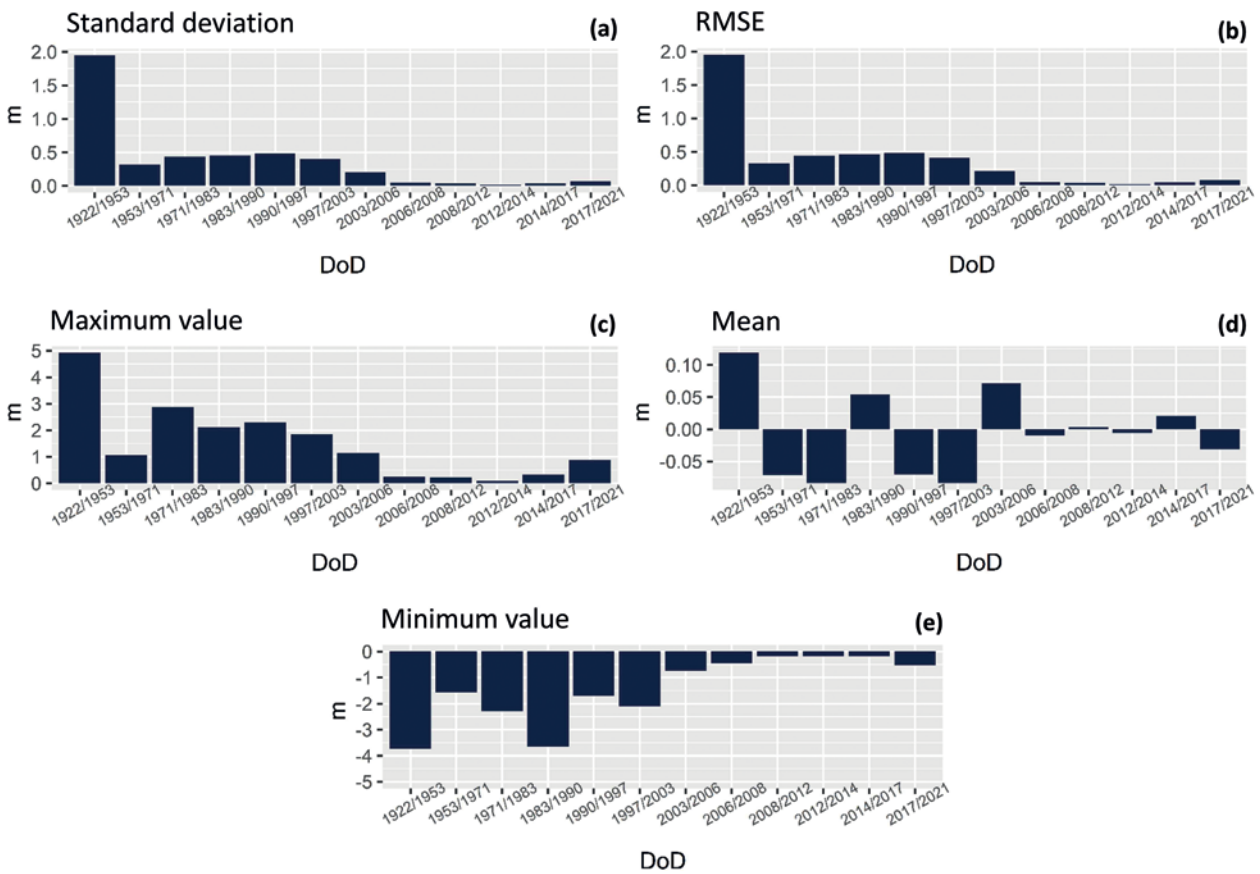

Fig. 4. Error assessment (based on the stable areas in Fig. 6).

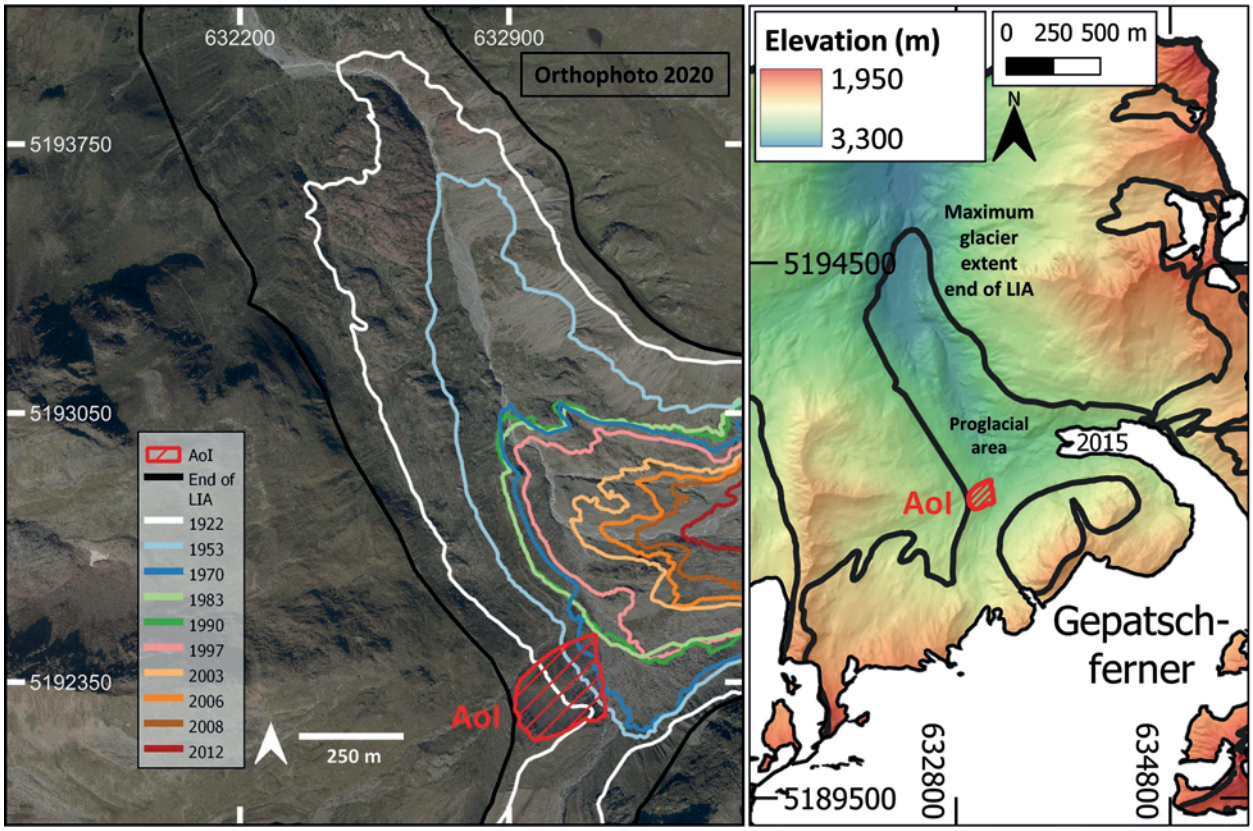

Fig. 5. Mapping of the glacier extents of the Gepatschferner with included AoI. Sources of the glacier extents: End of LIA: Groß & Patzelt (2015), 1922 to 2012: Own mapping by change detection analysis according to Abermann et al., (2010) based on DoDs (see sec. 3.2) (corresponding mapping method also includes mapping of debris-covered glacier parts) and 2015: Buckel & Otto (2018). Source of the orthophoto 2020: Province of Tyrol (Department of Geoinformation, Innsbruck, Austria).

in the interpolation of the contour lines of the 1922 DEM, which can occur especially in complex slope structures (Fleischer et al. 2022). Therefore, two different DEMs were created using the point cloud of 1953 and a corresponding DoD was created to compare the difference between the stable area and the AoI, which involves a much more complex terrain. First, a DEM (5×5 m) was created from the 1953 point cloud (point cloud to grid, aggregate Z, mean) and second, contour lines (20 m) were extracted from the 1953 point cloud and processed into a DEM accordingly (topo to raster, as described in section 3.2.1). The difference between the determined parameters once for the stable area and once of the AoI was used as correction factor. It is assumed that the topography of the AoI does not change when determining the correction factor, therefore the DEM of 1953 was used, as it shows the least changes compared to 1922. The calculated correction error was 1.24 and was multiplied by the error value calculated by Anderson (2019) (Fig. 7).

4 Results and discussion

4.1 Glacier mapping and long-term landslide monitoring from 1922 to 2021 (99 years)

The Gepatschferner retreated considerably since the end of the LIA. As a consequence, the AoI has been ice-free since at least 1980, as could be calculated based on the Euclidian distance (Betz-Nutz et al. 2022) between the two glacier extents of 1983 and 1990 (Fig. 5).

Based on the interpretation of the DoDs, the volume calculations and the profile lines (Figs 6, 7 and 8), the main slide of the lateral moraine deformation could be dated to the years between 1953 and 1971. In this epoch, the erosion area shows negative elevation changes of up to ~25 m, while the corresponding accumulation area assumes values of ~8 m (Fig. 6). However, a considerable part of the accumulation was probably already

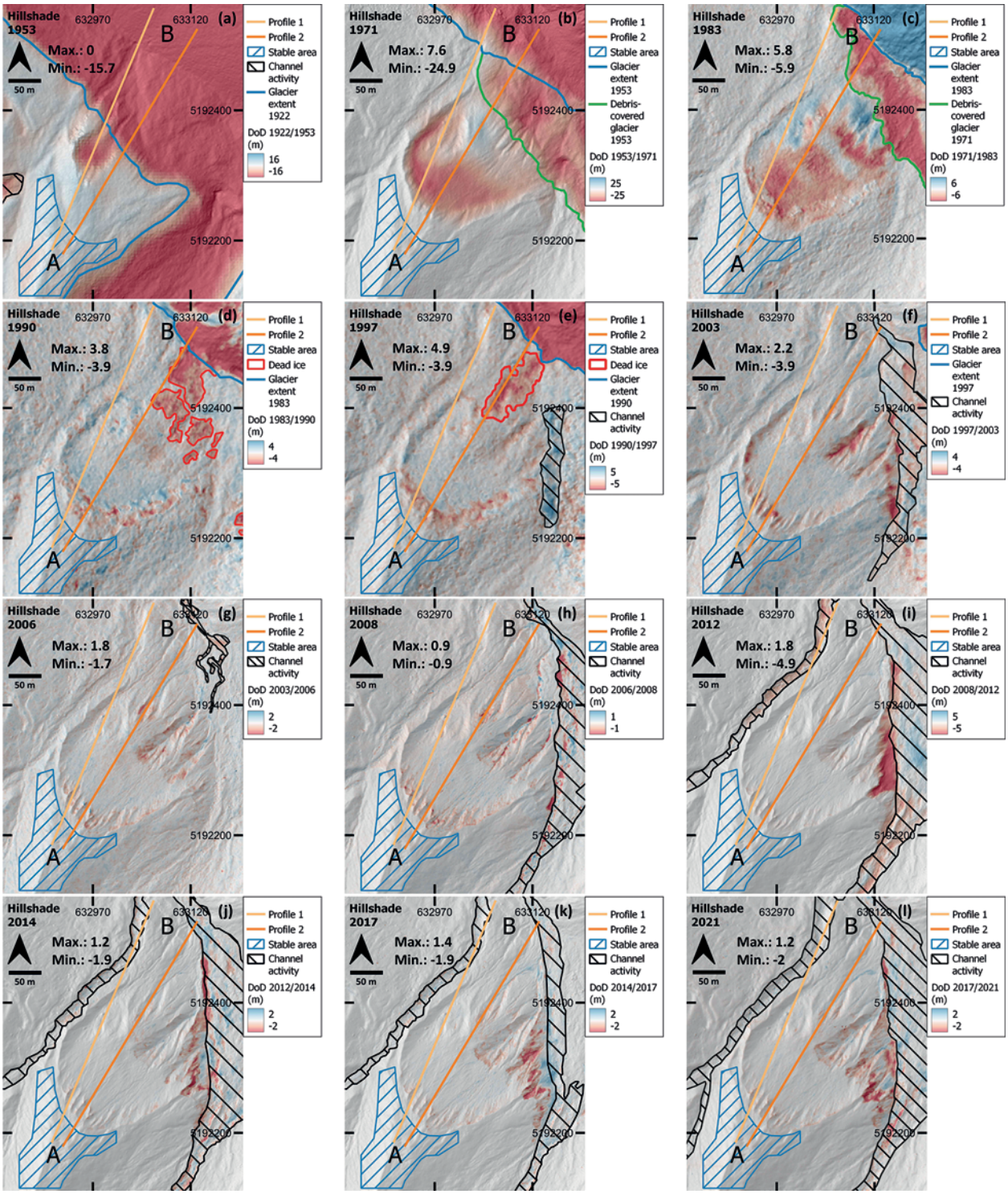

Fig. 6. Spatial and temporal visualisation **(a-l)** of the landslide area (DoD scale of each map is defined by the minimum or maximum of the variation of the AoI of the corresponding epoch, corresponding values are given – only geomorphological activity). The cross-sections of profile lines 1 and 2 (and profile directions A and B) are shown in Fig. 9.

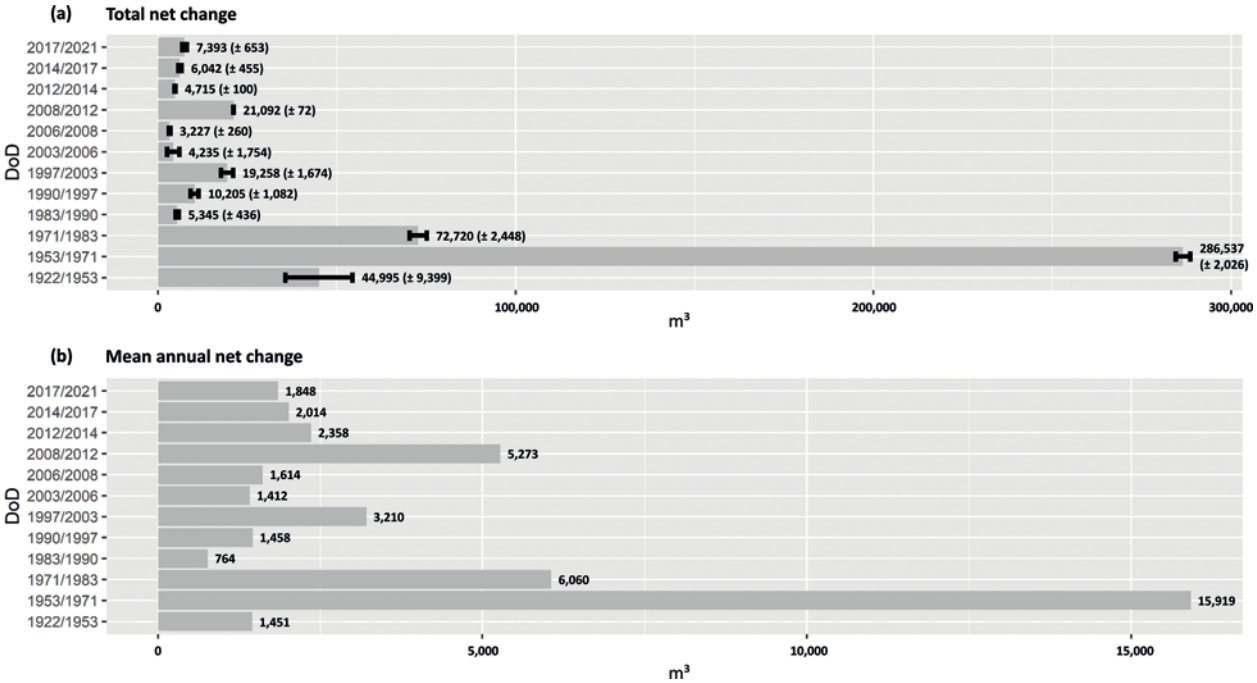

Fig. 7. Calculation of the **(a)** total and **(b)** mean annual net change of the epochs of the AoI.

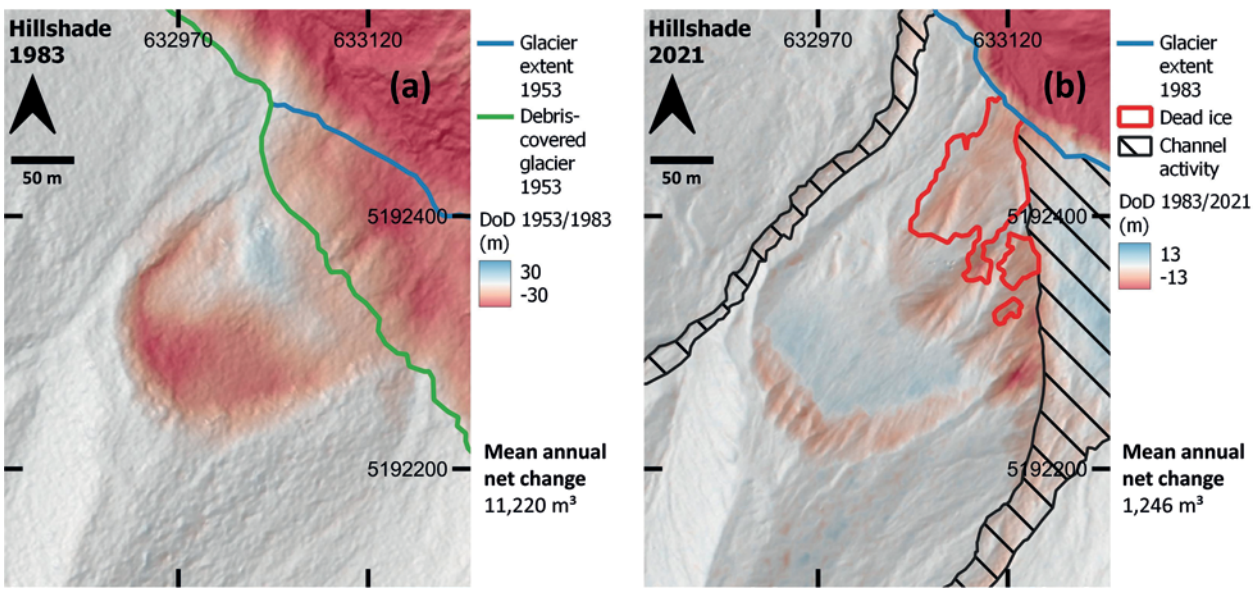

Fig. 8. Summary DoDs of the main periods, **(a)** mainly landslide processes and **(b)** mainly gully erosion and erosion on the eastern part of the AoI due to, e.g. slope undercutting. The DoD scale of each map is defined by the minimum and maximum of the variation of AoI of the corresponding epoch (only geomorphological activity). In **(b)**, the mapping of channel activity and dead ice is composed of the individual mappings from Fig. 6 (d-l).

transported downslope on the melting glacier, so that the accumulation area probably had higher values directly after the event. However, the first epoch (1922 to 1953) already shows a smaller slide in the upper part of the AoI, with maximum negative elevation changes of up to 16 m (Fig. 6). An interpretation of the contour lines of the historical map of 1886/1887 (Fig. 3) and the historical terrestrial oblique photo of 1890 (Fig. 1) also shows that there was no evidence of early deformation at these times. This is also indicated by the historic map of 1922, so we assume that no larger landslides occurred between the end of the LIA and 1886/1887, and between 1886/1887 and 1922. Within the period after the main slide (from 1971 to 1983) another landslide process with corresponding accumulation area could be detected, with negative and maximum height changes of up to 6 m (Fig. 6). Thus, different landslide processes could be reconstructed in the 61 years of the first three epochs (1922 to 1983), which, however, are difficult to separate from each other. In addition, based on DoD interpretation, a dead ice influence is very likely in the lower part of the slope until (max.) 1997. In the following decades, the zone of geomorphologically active areas within the AoI has changed considerably. Especially until 2008 (in the epochs 1983 to 1990, 1990 to 1997, 1997 to 2003, 2003 to 2006 and 2006 to 2008), high geomorphological activity can be identified in the upper area of the AoI, which led to the formation of a deeply incised gully system. From 2008 onwards, the geomorphological activity in the gully system is clearly lower. In the epochs from 2008 to 2021 (and from 1997 to 2003), a reworking of the eastern part of the slope is evident due to, e.g. the undercutting of the slope by the adjacent stream (Fagge river).

In addition, due to the different geomorphological processes, several epochs were summarised and corresponding DoDs were generated (Fig. 8). The period from 1953 to 1983 (30 years), which was mainly characterised by landslides, shows a mean annual net change of 11,220 m^3. The period from 1922 to 1953 was omitted because only minor changes were registered and a large part of the lateral moraine was still covered by ice. The second period from 1983 to 2021 (38 years), which was mainly characterised by gully erosion and morphodynamic of the eastern part of the AoI (volume of dead ice and channel activity were excluded), shows a mean annual net change of 1,246 m^3, which corresponds to a decrease of 89 %. If the previously calculated individual epochs (Fig. 7) are combined, the mean annual net change for the epoch 1953 to 1983 is 11,975 m^3 (deviation of 6.3 %) and for the epoch 1983 to 2021 2,145 m^3 (deviation of 41.9 %), which corresponds to a decrease of 82 %. This difference is due to the fact that several erosion areas between 1953 and 1983 are not included in the calculation (smaller area) and that the dead ice area in the second epoch from 1983 to 2021 is significantly smaller in the individual epochs (individual DoDs). Finally, we consider the summary of the calculation of the individual epochs to be less prone to error, so that we can assume a decrease in the mean annual net change of 11,975 m^3 (1953 to 1983) and of 2,145 m^3 (1983 to 2021), which corresponds to a decrease of 82 % and is mainly due to the different geomorphological processes.

Fig. 9 shows two profile lines from A to B (shown in Fig. 6). Profile line 1 mainly shows a cross profile of the area of the landslide within the first epoch (1922 to 1953) and profile line 2 shows a cross profile of the area of the second landslide (1953 to 1971), the main landslide (with corresponding enlargement of the headcut). In the epoch between 1953 and 1971, the main landslide has a width of about 190 m and a vertical and horizontal change of about 70 and about 100 m, respectively (Fig. 9). The close-up detail of the headcut shows a continuous retreat, although inaccuracies of the DEMs have also led to erroneous overlaps, especially of the 1922 DEM.

The AoI, as the terminal part of the lateral moraine, probably also has a special genesis, as in the corresponding area two outlets of the Gepatschferner were connected during the maximum glacier extent of the LIA (Figs 5 and 6), which probably allowed the formation of a correspondingly high lateral moraine and led to the accordingly large-scale deformation by glacial debuttressing. In this study, based on the reconstruction of the glacier extent as well as the corresponding morphodynamics, especially the landslides between 1922 and 1983, we assume a direct connection between the glacier retreat and the corresponding slope instability.

Compared to the landslide described by Hugenholtz et al. (2008) with a volume of about 900.000 m^3, the main landslide of this study (1953 to 1971) has a smaller width, but about twice the vertical and horizontal displacement and only a third of the volume of 286,537 (±2,026) m^3, whereby the total change over the entire time of almost 100 years is about half with ~486,000 m^3. However, the main deformations of both studies occurred at a similar time in the 1950s and 1960s. Mattson & Gardner (1991) detected a total of 25 mass wasting events, mainly rapid failures, in 1984 and 1985 in the glacier forefield of the Boundary glacier (Alberta, Canada). Most of them occurred during or immediately after rainfall events. However, the instability is generally due to the ice-core moraine. The estimated volume of all events totals 35,059 m^3, whereby the individual events range from 1 m^3 to 7,500 m^3, i.e. comparatively small events. The landslide in 2009 shown by Stoffel & Huggel (2012) with a volume of about 300,000 m^3 shows a similar erosion volume as the main deformation of this study between 1953 and 1971. The 25 landslides, shown by Emmer et al. (2020) (in the glacier forefield of Kinzl

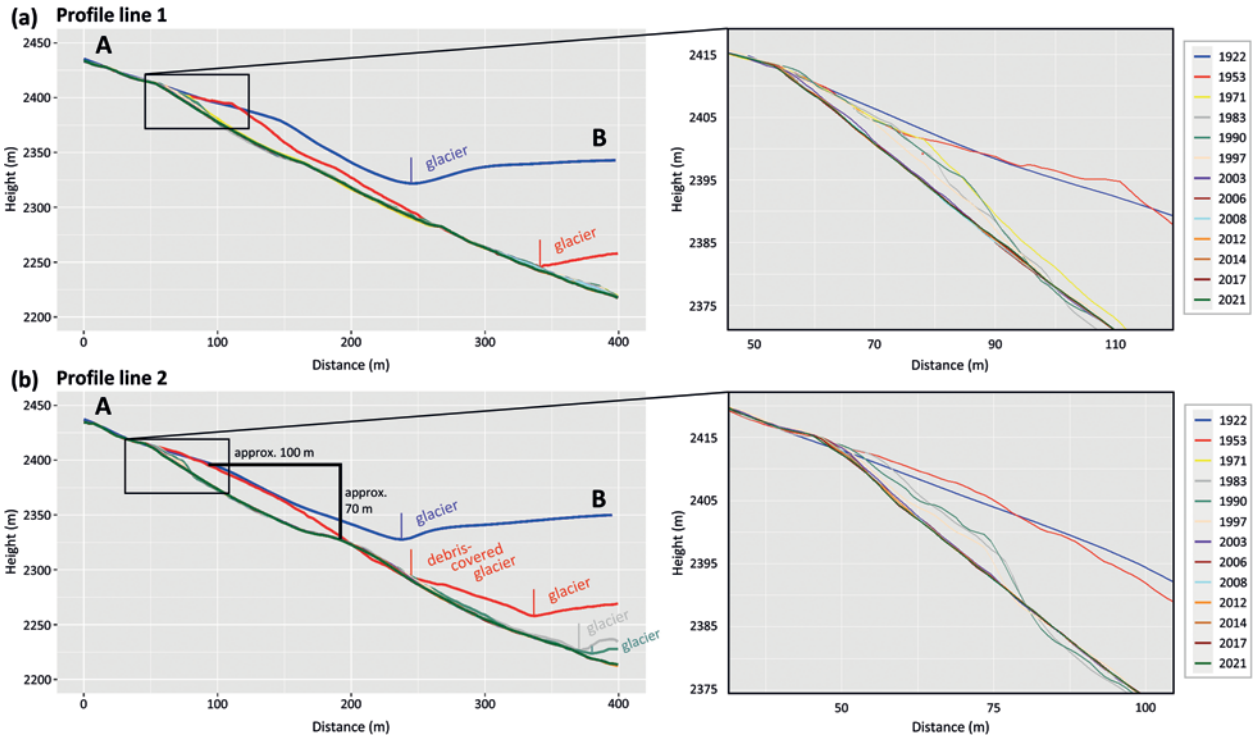

Fig. 9. Profile line 1 **(a)** and 2 **(b)** of the landslide and corresponding enlargement of the headcut (20 m swath profile) (Profile line 1 and 2 shown in Fig. 6, A and B show the direction).

Glacier, Peruvian Cordillera Blanca), which are directly or indirectly attributable to the glacier retreat, have a total area of 410,072 m^2 with a total erosion volume of 10^6 m^3.

However, no statement can be made about the velocity of the landslides, so that it may have been slow, as shown for example by Cody et al. (2020), or fast and sudden slope deformations. As in Cody et al. (2020), it could be shown that landslides are the dominant process during the ice-freeing of the slope. Nevertheless, it can be seen that after the landslides (1922 to 1983) there is a continuous geomorphological activity, with a total of almost 100 years. Due to changes in the type of geomorphological processes in the different epochs, there is also considerable variability in the volume detection of these. In the decades after the landslides, a gully system has formed, presumably due to fluvial and nival erosional processes, slope wash, slope failures and debris flows as shown by Ballantyne (2002b) and Curry et al. (2006). The monitoring of the slope does not indicate a stabilisation of the slope, although the erosion volume has decreased considerably, which is mainly due to the change in the geomorphological processes. Piermattei et al. (2022) showed that a considerable amount of the sediment provided by this slope has reached the adjacent river (Fagge) in recent decades, where it partly accumulated.

4.2 Uncertainty of the historical map, SfM-MVS photogrammetric and LiDAR based DEMs

The approach of combining DEMs from historical maps (1886/1887 and 1922) with subsequent DEMs from aerial photographs (by SfM-MVS photogrammetry) and airborne LiDAR data (Light detection and ranging) (from the middle of the 20th century to the present) shows that this is partially suitable to extend the temporal aspect of (3D) volume change detection of geomorphological slope processes in glacier forefields by several decades. While the stereo photogrammetric map of 1922 (Finsterwalder 1928) was well suited for the corresponding analysis, it also turned out that the 1886/1887 map (Finsterwalder & Schunck 1888), which is based on trigonometric measurements with a theodolite (as well as photos and terrain sketches), has too high inaccuracies for a change detection analysis, as there was a shift of the contour lines by several tens of metres around the AoI (not in the measured points in the entire map). These inaccuracies are surely the result of the interpolation of the less measurement points to contour lines. Nevertheless the 1886/1887 map provides a good picture of the general conditions on and around the AoI and thus can help to understand the geomorphodynamic in this area.

The DEM generated from the 1922 map has some inaccuracies that are difficult to quantify, e.g. due to scanning biases or georeferencing of the map to the contour lines of the 2017 DEM. With 305 clearly identifiable and evenly distributed co-registration points, an usable georeferencing was implemented. In addition, uncertainties arise from the stereo photogrammetric processing of the map, such as the positioning of the photo locations in the field. In this case, Finsterwalder (1928) gives a mean positional accuracy of the photo locations in xy-direction of 0.5 m and a height of 0.3 m. Further uncertainties arise from the large-scale interpolation of the 20 m contour lines. Finally, Fig. 4 shows that the highest uncertainties are found in the 1922 DEM, which also leads to the highest estimated volume error (DoD 1922/1953), which are shown in Fig. 7. Furthermore, it can be seen that the error estimates of DEMs based on airborne LiDAR are also lower compared to DEMs based on aerial photos (SfM photogrammetry), which shows a continuous improvement in the accuracy of surveying the Earth's surface. While the RMSE for the 1922 DEM is 1.95 m, it averages 0.39 m for DEMs generated from aerial images (SfM photogrammetry) (1953 to 2003) and 0.04 m for airborne LiDAR DEMs (2006 to 2021). However, in the case of correspondingly large topographic changes (e.g. landslides), it is quite possible to quantify corresponding changes in the Earth's surface using historical maps, which extends the period of investigation by several decades.

5 Conclusion

In this study, a large-scale landslide at the terminal part of a LIA lateral moraine was investigated. The aim was to combine different topographic data sets from different epochs and thus also based on different remote sensing techniques in order to ensure the longest possible quantitative study period by calculating volume changes of the Earth's surface. Thus, from current LiDAR (2006 to 2021) and historical photogrammetric (aerial photographs from 1953 to 2003) based DEMs, it was also possible to generate a DEM from a stereo photogrammetric map from 1922, ensuring an observation period of almost 100 years. This study thus shows how useful it is to combine different topographic datasets from different epochs, as this allows longer study periods, extending the monitoring of high alpine areas by several decades into the first half of the 20th century. The extension of the study period thus also means that the paraglacial adjustment process of proglacial areas can already be analysed quantitatively several decades before the middle of the 20th century and thus, in addition, earlier slope processes can also be determined, which is a clear advantage over previous studies. In the first three epochs (in total from 1922 to 1983), several landslides could be quantified and interpreted, whereby the second epoch from 1953 to 1971 represents the period with the largest deformation. The landslides correspond in time to the (almost) continuous glacier retreat, so that we assume the landslides to be a direct consequence of the glacial debuttressing caused by the glacier retreat. In the following epochs, a reworking of the deformation could be observed, so that a continuous geomorphological activity can be described and single geomorphic processes could be distinguished over the entire investigation period of almost 100 years. The gully system shows a persisting geomorphological activity, especially until 2008. Between 2008 and 2021 (and 1997 to 2003), a reworking of the eastern part could be observed, probably due to the slope undercutting of the adjacent river, as sediment activity within the channel can also be observed during these epochs. This shows that the reworking of lateral moraines is on the one hand a process, which is governed by different geomorphic processes and a steady decline of geomorphic activity, but that such a steady state could be disturbed by e.g. a single process like undercutting. The comparison with similar studies shows that surveys about large-scale landslides of lateral moraines are very rare and that special conditions were present in each case. In this case, the formation of the lateral moraine probably also plays a role, because the interconnection of two different outlets of the Gepatsch glacier led to a correspondingly large formation of the terminal part of the lateral moraine, which lost stability due to the retreat of the glacier. Beside this, no other studies used historical maps for a quantitative analysis of morphological changes over an investigation period of almost 100 years. However, due to the higher uncertainties of the historical map-based DEMs compared to the photogrammetric and LiDAR-based DEMs, only major topographic changes can probably be quantified and interpreted within the corresponding epoch. However, the study shows that historical maps are well suited to extend the monitoring of proglacial areas in time, so we encourage scientists to search for further historical maps and to carry out corresponding morphodynamic analyses in order to get a better picture of long-term changes in proglacial areas.

Competing interests: All authors declare that they have no conflicts of interest.Fundingand

Funding and Acknowledgements: The study is part of the SEHAG project ("Sensitivity of High Alpine Geosystems

to Climate Change Since 1850"), which was funded by the Deutsche Forschungsgemeinschaft (DFG, German Research Foundation; project number 394200609) and the Austrian Science Fund (FWF), for which we would like to express our gratitude. We would also like to thank the Federal Office of Metrology and Surveying (BEV, Vienna, Austria) and the Province of Tyrol (Department of Geoinformation, Innsbruck, Austria) for providing the historical aerial photographs. In addition, we would like to thank the pioneers of surveying high alpine areas, e.g. S. Finsterwalder, H. Schunck, A. Blümcke, S. Ulrich, R. Finsterwalder and J. Sartorius, who made a correspondingly long survey period in the Upper Kaunertal possible. Additionally, we thank the two anonymous reviewers for the constructive comments which significantly helped to improve the manuscript. The open access publication of this article was supported by the Open Access Fund of the Catholic University of Eichstätt-Ingolstadt.

References

Abermann, J., Fischer, A., Lambrecht, A., & Geist, T. (2010). On the potential of very high-resolution repeat DEMs in glacial and periglacial environments. *The Cryosphere, 4*(1), 53–65. https://doi.org/10.5194/tc-4-53-2010

Altmann, M., Piermattei, L., Haas, F., Heckmann, T., Fleischer, F., Rom, J., … Becht, M. (2020). Long-Term Changes of Morphodynamics on Little Ice Age Lateral Moraines and the Resulting Sediment Transfer into Mountain Streams in the Upper Kauner Valley, Austria. *Water (Basel), 12*(12), 3375. https://doi.org/10.3390/w12123375

Altmann, M., Pfeiffer, M., Haas, F., Rom, J., Fleischer, F., Heckmann, T., … Becht, M. (2023). Long-term monitoring (1953–2019) of geomorphologically active sections on LIA lateral moraines under changing meteorological conditions. EGUsphere [Preprint], https://doi.Org/10.5194/egusphere-2022-1512

Anderson, S. W. (2019). Uncertainty in quantitative analyses of topographic change: Error propagation and the role of thresholding. *Earth Surface Processes and Landforms, 44*(5), 1015–1033. https://doi.org/10.1002/esp.4551

Bakker, M., & Lane, S. (2017). Archival photogrammetric analysis of river-floodplain systems using Structure from Motion (SfM) methods. *Earth Surface Processes and Landforms, 42*(8), 1274–1286. https://doi.org/10.1002/esp.4085

Ballantyne, C. K. (2002a). A general model of paraglacial landscape response. *The Holocene, 12*(3), 371–376. https://doi.org/10.1191/0959683602hl553fa

Ballantyne, C. K. (2002b). Paraglacial geomorphology. *Quaternary Science Reviews, 21*(18-19), 1935–2017. https://doi.org/10.1016/S0277-3791(02)00005-7

Ballantyne, C. K., & Benn, D. I. (1994). Paraglacial Slope Adjustment and Resedimentation following Recent Glacier Retreat, Fåbergstølsdalen, Norway. *Arctic and Alpine Research, 26*(3), 255–269. https://doi.org/10.2307/1551938

Besl, P. J., & McKay, N. D. (1992). Method for registration of 3-D shapes. In P. S. Schenker (Ed.), *SPIE Proceedings, Sensor Fusion IV: Control Paradigms and Data Structures* (pp. 586–606). SPIE. https://doi.org/10.1117/12.57955

Betz-Nutz, S., Heckmann, T., Haas, F., & Becht, M. (2023). Development of the morphodynamics on Little Ice Age lateral moraines in 10 glacier forefields of the Eastern Alps since the 1950s. *Earth Surface Dynamics, 11*(2), 203–226. https://doi.org/10.5194/esurf-11-203-2023

Blair, R. W. (1994). Moraine and Valley Wall Collapse due to Rapid Deglaciation in Mount Cook National Park, New Zealand. *Mountain Research and Development, 14*(4), 347. https://doi.org/10.2307/3673731

Bollmann, E., Sailer, R., Briese, C., Stötter, J., & Fritzmann, P. (2011). Potential of airborne laser scanning for geomorphologic feature and process detection and quantifications in high alpine mountains. *Zeitschrift für Geomorphologie, 55*(2), 83–104. https://doi.org/10.1127/0372-8854/2011/0055S2-0047

Buckel, J., & Otto, J.-C. (2018). The Austrian Glacier Inventory GI 4(2015) in ArcGis (shapefile) format, supplement to: Buckel, Johannes; Otto, Jan-Christoph; Prasicek, Günther; Keuschnig, Markus (2018): Glacial lakes in Austria – Distribution and formation since the Little Ice Age. Global and Planetary Change, 164, 39–51. PANGAEA – Data Publisher for Earth & Environmental Science. https://doi.org/10.1594/PANGAEA.887415

Cody, E., Anderson, B. M., McColl, S. T., Fuller, I. C., & Purdie, H. L. (2020). Paraglacial adjustment of sediment slopes during and immediately after glacial debuttressing. *Geomorphology, 371*, 107411. https://doi.org/10.1016/j.geomorph.2020.107411

Copernicus (2016). Hillshade derived from EU-DEM version 1.0. Retrieved from https://land.copernicus.eu/imagery-in-situ/eu-dem/eu-dem-v1-0-and-derived-products/hillshade?tab=metadata

Curry, A. M., Cleasby, V., & Zukowskyj, P. (2006). Paraglacial response of steep, sediment-mantled slopes to post-'Little Ice Age' glacier recession in the central Swiss Alps. *Journal of Quaternary Science, 21*(3), 211–225. https://doi.org/10.1002/jqs.954

Deline, P., Gruber, S., Delaloye, R., Fischer, L., Geertsema, M., Giardino, M., & Schoeneich, P. (2015). Ice Loss and Slope Stability in High-Mountain Regions. In W. Haeberli, C. Whiteman, & J. F. Shroder (Eds.), *Hazards and disasters series. Snow and ice-related hazards, risks, and disasters* (pp. 521–561). Amsterdam: Elsevier; https://doi.org/10.1016/B978-0-12-394849-6.00015-9

Emmer, A., Klimeš, J., Hölbling, D., Abad, L., Draebing, D., Skalák, P., … Zahradníček, P. (2020). Distinct types of landslides in moraines associated with the post-LIA glacier thinning: Observations from the Kinzl Glacier, Huascarán, Peru. *The Science of the Total Environment, 739*, 139997. https://doi.org/10.1016/j.scitotenv.2020.139997

Finsterwalder, S. (1928). Begleitworte zur Karte des Gepatschferners. *Zeitschrift für Gletscherkunde, XVI*(1/2), 20–41.

Finsterwalder, S., & Schunck, H. (1888). Die Zunge des Gepatschferners 1886/87. *Zeitschrift Des Deutschen Und Oesterreichischen Alpenvereins*, Tafel 4.

Fleischer, F., Haas, F., Altmann, M., Rom, J., Knoflach, B., & Becht, M. (2022). Combination of historical and modern data to decipher the geomorphic evolution of the Innere Ölgruben rock glacier, Kaunertal, Austria, over almost

a century (1922–2021). *Permafrost and Periglacial Processes*; Advance online publication. https://doi.org/10.1002/ppp.2178

Fleischer, F., Haas, F., Piermattei, L., Pfeiffer, M., Heckmann, T., Altmann, M., … Becht, M. (2021). Multi-decadal (1953–2017) rock glacier kinematics analysed by high-resolution topographic data in the upper Kaunertal, Austria. *The Cryosphere, 15*(12), 5345–5369. https://doi.org/10.5194/tc-15-5345-2021

Geological Survey of Austria (1999). Geological map of Austria, 1:2.000.000. Vienna.

Groß, G., & Patzelt, G. (2015). The Austrian Glacier Inventory for the Little Ice Age Maximum (GI LIA) in ArcGIS (shapefile) format. PANGAEA – Data Publisher for Earth & Environmental Science. https://doi.org/10.1594/PANGAEA.844987

Guo, C., Xu, Q., Dong, X., Li, W., Zhao, K., Lu, H., & Ju, Y. (2021). Geohazard Recognition and Inventory Mapping Using Airborne LiDAR Data in Complex Mountainous Areas. *Journal of Earth Science, 32*(5), 1079–1091. https://doi.org/10.1007/s12583-021-1467-2

Haeberli, W., Schaub, Y., & Huggel, C. (2017). Increasing risks related to landslides from degrading permafrost into new lakes in de-glaciating mountain ranges. *Geomorphology, 293*, 405–417. https://doi.org/10.1016/j.geomorph.2016.02.009

Heckmann, T., & Morche, D. (Eds.). (2019). *Geography of the Physical Environment. Geomorphology of proglacial systems: Landform and sediment dynamics in recently deglaciated alpine landscapes*. Cham, Switzerland: Springer. https://doi.org/10.1007/978-3-319-94184-4

Hilger, L. (2017). *Quantification and regionalization of geomorphic processes using spatial models and high-resolution topographic data: A sediment budget of the Upper Kauner Valley, Ötztal Alps*. (Doctoral thesis). Catholic University of Eichstätt-Ingolstadt, Eichstätt.

Hock, R., Rasul, G., Adler, C., Cáceres, B., Gruber, S., Hirabayashi, Y.: Jackson, M., … Milner, A. L. (2019). High Mountain Areas: In: H.-O. Pörtner, D.C. Roberts, V. Masson-Delmotte, P. Zhai, M. Tignor, E. Poloczanska, K. Mintenbeck, A. Alegría, M. Nicolai, A. Okem, J. Petzold, B. Rama, N.M. Weyer (eds.), *IPCC Special Report on the Ocean and Cryosphere in a Changing Climate* (pp. 131–202). Cambridge, UK and New York, NY, USA: Cambridge University Press. https://doi.org/10.1017/9781009157964.004

Hugenholtz, C. H., Moorman, B. J., Barlow, J., & Wainstein, P. A. (2008). Large-scale moraine deformation at the Athabasca Glacier, Jasper National Park, Alberta, Canada. *Landslides, 5*(3), 251–260. https://doi.org/10.1007/s10346-008-0116-5

Ivy-Ochs, S., Kerschner, H., Maisch, M., Christl, M., Kubik, P. W., & Schlüchter, C. (2009). Latest Pleistocene and Holocene glacier variations in the European Alps. *Quaternary Science Reviews, 28*(21-22), 2137–2149. https://doi.org/10.1016/j.quascirev.2009.03.009

James, L. A., Hodgson, M. E., Ghoshal, S., & Latiolais, M. M. (2012). Geomorphic change detection using historic maps and DEM differencing: The temporal dimension of geospatial analysis. *Geomorphology, 137*(1), 181–198. https://doi.org/10.1016/j.geomorph.2010.10.039

Lane, S., Bakker, M., Gabbud, C., Micheletti, N., & Saugy, J.-N. (2017). Sediment export, transient landscape response and catchment-scale connectivity following rapid climate warming and Alpine glacier recession. *Geomorphology, 277*, 210–227. https://doi.org/10.1016/j.geomorph.2016.02.015

Matthews, J. A., & Briffa, K. R. (2005). The 'little ice age': Re-evaluation of an evolving concept. *Geografiska Annaler. Series A. Physical Geography, 87*(1), 17–36. https://doi.org/10.1111/j.0435-3676.2005.00242.x

Mattson, L. E., & Gardner, J. S. (1991). Mass Wasting on Valley-Side Ice-Cored Moraines, Boundary Glacier, Alberta, Canada. *Geografiska Annaler. Series A. Physical Geography, 73*(3-4), 123–128. https://doi.org/10.1080/04353676.1991.11880337

McNabb, R. (2019). pybob: https://github.com/iamdonovan/pybob/tree/44467f670811548c4cabaa5c29eb4b6a66615a6d, last access: 06.05.2021.

Midgley, N. G., & Tonkin, T. N. (2017). Reconstruction of former glacier surface topography from archive oblique aerial images. *Geomorphology, 282*, 18–26. https://doi.org/10.1016/j.geomorph.2017.01.008

Nicolussi, K., & Kerschner, H. (2014). Lateglacial and Holocene advance record of the Gepatschferner, Kaunertal, Tyrol. From the foreland to the Central Alps. Field Trips to selected sites of Quaternary research in the Tyrolean and Bavarian Alps. In H. Kerschner, K. Krainer, & C. Spötl (Eds.), (pp. 144–151). Berlin: Geozon.

Nicolussi, K., & Patzelt, G. (2001). Untersuchungen zur holozänen Gletscherentwicklung von Pasterze und Gepatschferner (Ostalpen). *Zeitschrift für Gletscherkunde und Glazialgeologie, 36*, 1–88.

Piermattei, L., Heckmann, T., Betz-Nutz, S., Altmann, M., Rom, J., Fleischer, F., … Becht, M. (2022). Evolution of an Alpine proglacial river during seven decades of deglaciation quantified from photogrammetric and LiDAR digital elevation models. [Preprint]. *Earth Surface Dynamics Discussions*; Advance online publication. https://doi.org/10.5194/esurf-2022-63

Sailer, R., Bollmann, E., Hoinkes, S., Rieg, L., Sproß, M., & Stötter, J. (2012). Quantification of geomorphodynamics in glaciated and recently deglaciated terrain based on airborne laser scanning data. *Geografiska Annaler. Series A. Physical Geography, 94*(1), 17–32. https://doi.org/10.1111/j.1468-0459.2012.00456.x

Schiefer, E., & Gilbert, R. (2007). Reconstructing morphometric change in a proglacial landscape using historical aerial photography and automated DEM generation. *Geomorphology, 88*(1-2), 167–178. https://doi.org/10.1016/j.geomorph.2006.11.003

Stark, M., Rom, J., Haas, F., Piermattei, L., Fleischer, F., Altmann, M., & Becht, M. (2022). Long-term assessment of terrain changes and calculation of erosion rates in an alpine catchment based on SfM-MVS processing of historical aerial images. How camera information and processing strategy affect quantitative analysis. *Journal of Geomorphology*. Advance online publication. https://doi.org/10.1127/jgeomorphology/2022/0755

Stoffel, M., Tiranti, D., & Huggel, C. (2014). Climate change impacts on mass movements – Case studies from the

European Alps. *The Science of the Total Environment, 493*, 1255–1266. https://doi.org/10.1016/j.scitotenv.2014.02.102

Stoffel, M., & Huggel, C. (2012). Effects of climate change on mass movements in mountain environments. *Progress in Physical Geography, 36*(3), 421–439. https://doi.org/10.1177/0309133312441010

Williams, R. (2012). Dems of difference. *Geomorphological Techniques, 2(3.2)*. Retrieved from https://eprints.gla.ac.uk/114527/

Manuscript received: December 20, 2022
Revisions requested: January 28, 2023
Revised version received: February 26, 2023
Accepted: March 22, 2023